Transactions **of the SMiRT 27**
Yokohama, Japan, March 3-8, 2024
Division V

ISOLATED FUEL STORAGE POOL SEISMIC BEHAVIOR – EFFECT OF FLUID AND ISOLATORS MODELING

Nadim Moussallam[1], Simon Lehmann[2], Nicolas Besson[3]

[1] Expert engineer, Framatome, Lyon France (nadim.noussallam@framatome.com)
[2] Specialist engineer, Framatome, Lyon France
[3] Expert engineer, EDF, Lyon France

ABSTRACT

In the nuclear industry, large concrete pools are used for the long-term storage of spent fuel assemblies after their use in reactor. The largest of these structures are sometimes supported on soft pads, or isolators, that can simultaneously allow a free thermal expansion of the pool concrete and dynamically isolate the pool from possible seismic excitations.

This paper gives the lessons learned from the seismic analysis of a fully coupled fluid-structure Finite Element (FE) model of a seismically isolated storage pool. The model set up and checking is described. Several dynamic coupling effects are highlighted, that influence the accelerations within the pool when compared to more standard industrial practices.

INTRODUCTION

Long term spent fuel storage pools are large concrete civil structures, typically several tenth of meters wide and possibly up to 100 m long, that support racks or baskets of fuel assemblies stored under water. They are designed to maintain a constant cooling and water cover of the fuel assemblies. Because the temperature of the inner water might be higher than the external varying ambient temperature, and because of the large dimensions of the pool, a significant thermal expansion of the pool relative to its host building foundation shall be accommodated. Implementing a soft layer of pads or isolators between the pool and its foundation allows such an accommodation.

The adjunction of a soft layer between the pool and its foundation also allows to seismically isolate the pool from the ground accelerations and thus reduce the dynamic excitation experienced by its equipment: the fuel racks or basket resting on the pool bottom but also the cooling systems and the handling machineries attached to the pool concrete walls. Several technologies of isolators have been implemented below large fuel storage pools including elastomeric rubber bearings (see AFCEN 2014 and Moussallam 2013) and 3D spring-dampers systems (see Nawrotzki 2019). The elastomeric rubber bearings work essentially in the horizontal plane, decreasing the horizontal response frequencies of the pool. The 3D spring-damper systems decrease both the in-plane and the vertical response frequencies of the isolated structure. In this case coupled modes exist, combining vertical and horizontal movements of the isolated pool.

The present paper describes the lessons learned from the numerical simulation of the seismic response of a storage pool supported on 3D spring-damper systems. Some of these lessons are equally applicable to other kind of seismic isolation systems.

MODELING

Structural part

The isolated fuel storage pool, used as example in the present paper, is a rectangular shaped pool resting on a 3D spring-dampers isolation system. It is a reinforced concrete structure constituted of a bottom slab and lateral walls. A finite element modelling of this structure is presented in Figure 1 a). The structure is represented by shell and mass elements. The isolation system is represented by 2-nodes springs and damper elements connecting the pool bottom to its host building foundation. The overall seismic response of such system to a seismic excitation is defined by the discretized equation of dynamics:

$$\boldsymbol{M\ddot{u} + C\dot{u} + Ku = -M\ddot{u}_g} \qquad (1)$$

with $\boldsymbol{M}$, $\boldsymbol{C}$ and $\boldsymbol{K}$ respectively the mass, damping and stiffness matrices associated to the finite element model, $\boldsymbol{u}$ the vector of nodal displacements relative to the ground and $\boldsymbol{\ddot{u}_g}$ the vector of seismic excitation at the ground. One particular aspect of the $\boldsymbol{C}$ matrix of equation (1), in the case of a highly damped seismic isolation system, is that it comprises high value terms at the degrees of freedom attached to the viscous dampers. These localized high damping terms make the projection of equation (1) into the modal basis $\boldsymbol{\phi}$ impractical, as it would result in a non-diagonal $\boldsymbol{\phi^T C \phi}$ matrix.

Fluid part and coupled equation

The fluid inside the pool is considered at rest before the earthquake starts. No significant fluid flow is considered, be it before, during or after the earthquake. The viscous and turbulent effects in the fluid are also neglected. This last hypothesis is considered conservative since turbulence and viscosity do generally remove energy from the structural seismic response. The full Navier-Stokes equations describing the fluid behavior are reduced to the wave propagation equation inside a compressible fluid volume (2) associated with a pressure boundary condition at the interfaces with structures (3):

$$\boldsymbol{\nabla}\left(\frac{1}{\rho_0}\boldsymbol{\nabla} p\right) = \frac{1}{\rho_0 c^2}\frac{\partial^2 p}{\partial t^2} \qquad (2) \qquad\qquad \boldsymbol{n}.\boldsymbol{\nabla} p = -\rho_0 \boldsymbol{n}.\frac{\partial^2 \boldsymbol{u_a}}{\partial t^2} \qquad (3)$$

with p the pressure, c the celerity of sound within the fluid, $\boldsymbol{\nabla} p$ the pressure gradient vector at the fluid-structure interface, $\boldsymbol{n}$ a vector denoting the direction normal to the interface, $\boldsymbol{u_a}$ the absolute displacement vector of the fluid at the structure interface and ρ_0 the mean fluid density.

The introduction of these equations into a structural model can be achieved through purely acoustic finite elements, with pressure degrees of freedom at all nodes and displacement degrees of freedom at the nodes located on interfaces with the structure only. Using pressure based finite elements, the forces applied by the fluid on the structure at the interface are computed by:

$$\boldsymbol{F_{fluid} = RP} \qquad (4)$$

with $\boldsymbol{P}$ the vector of nodal pressures and the matrix $\boldsymbol{R}$ representing the discretization of the integral of the fluid pressure on the interface. The finite element modelling of the fluid within the pool is illustrated in Figure 1 b). The wave propagation equation (2) associated to the fluid-structure boundary condition equation (3) can be discretized in the following form:

$$\boldsymbol{M_F P + K_F \ddot{P} = -\rho_0 R^T \ddot{u}_{a,F}} \qquad (5)$$

The matrices $\boldsymbol{M_F}$ and $\boldsymbol{K_F}$ are obtained by discretization of the integral form of equation (2) and $\boldsymbol{\ddot{u}_{a,F}}$ represents the absolute acceleration vector of the fluid-structure interface nodes. This absolute acceleration can be decomposed into its relative part $\boldsymbol{\ddot{u}_{,F}}$ and the ground acceleration part $\boldsymbol{\ddot{u}_{g,F}}$. The

overall discrete dynamic equation of both the discretized fluid and the discretized structural system can be assembled in a single matrix equation with a form similar to equation (1):

$$\begin{bmatrix} \boldsymbol{M} & \boldsymbol{0} \\ \rho_0 \boldsymbol{R}^T & \boldsymbol{M_F} \end{bmatrix} \begin{Bmatrix} \ddot{\boldsymbol{u}} \\ \ddot{\boldsymbol{P}} \end{Bmatrix} + \begin{bmatrix} \boldsymbol{C} & \boldsymbol{0} \\ \boldsymbol{0} & \boldsymbol{0} \end{bmatrix} \begin{Bmatrix} \dot{\boldsymbol{u}} \\ \dot{\boldsymbol{P}} \end{Bmatrix} + \begin{bmatrix} \boldsymbol{K} & -\boldsymbol{R} \\ \boldsymbol{0} & \boldsymbol{K_F} \end{bmatrix} \begin{Bmatrix} \boldsymbol{u} \\ \boldsymbol{P} \end{Bmatrix} = \begin{Bmatrix} -\boldsymbol{M}\ddot{\boldsymbol{u}}_{\boldsymbol{g}} \\ -\rho_0 \boldsymbol{R}^T \ddot{\boldsymbol{u}}_{g,F} \end{Bmatrix} \qquad (6)$$

Unlike those of equation (1), the matrices of equation (6) are no longer symmetrical. The procedures used for determining the Eigen frequencies, the Eigen vectors and the coefficient of participation are then adapted.

Free fluid surface and sloshing modes

At the free surface of the fluid volume of Figure 1 b), sloshing phenomena (water waves) can be induced by the seismic motion. At any given point of the fluid surface and at any given time, the pressure p will be related to the wave height η at this given location by the equation:

$$p = \rho_0 g \eta \qquad (7)$$

with g the gravity acceleration. Here, the compressibility of the fluid is neglected for the representation of sloshing modes. Equation (7) is reproduced within the finite element model by setting up a fluid-structure boundary on the free surface of the fluid and connecting it to series of springs acting in the vertical direction and developing a vertical force proportional to η (local relative u_z displacement). The setup of these springs is represented in Figure 1 c). For a regular rectangular shape of pool, references such as Housner 1957 and, more recently, the Eurocodes give theoretical formula for computing the eigen frequencies of the main sloshing modes along each of the two horizontal directions separately:

$$f_n = \frac{1}{2\pi} \sqrt{\frac{n\pi g}{2l} \tanh\left(\frac{n\pi h}{2l}\right)} \qquad (8)$$

with f_n the eigen frequency of the nth sloshing mode taken within {1, 3, 5, …}, the half-length of the pool in the direction of interest and h the water height.

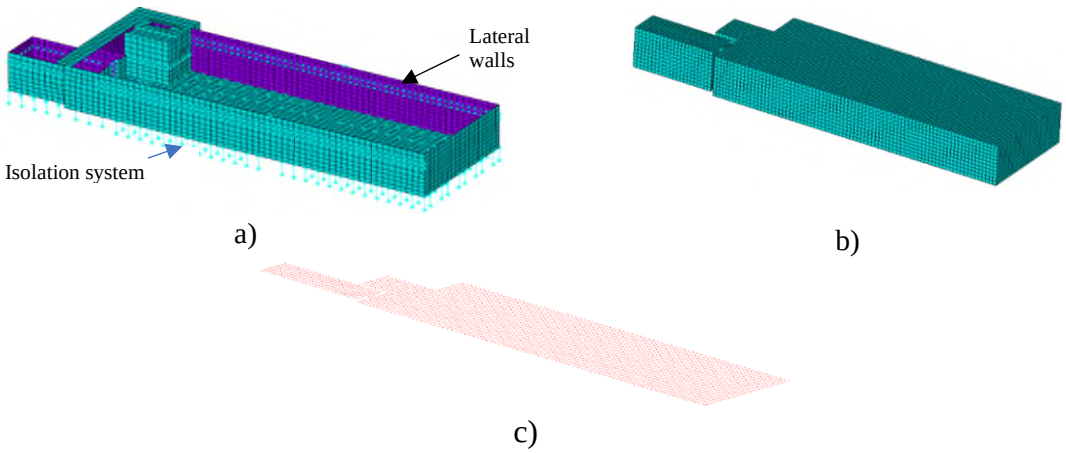

Figure 1. Finite element model of the pool – a) structural part b) fluid part and c) free surface springs

A first check of the free fluid surface modelling is performed using a regular rectangular pool model and comparing its modal analysis results with the theoretical formulation of equation (8). This comparison is given in Table 1 for the first eigen frequencies. It shows that the calculated modes are first fully aligned with the theory and then slightly drift away from it. Indeed, as the modes order increase, coupled X and Y direction sloshing mode appear that cannot be predicted by equation (8). Also, for higher order modes, the mesh size plays a role and ultimately limit the precision of the

calculated modes shape and frequency. Finally, for higher order modes, some couplings appear between the sloshing modes and the lateral wall modes of the pool.

n	1	3	5	7
fx (Hz)	0.19	0.28	0.34	0.40
fy (Hz)	0.22	0.32	0.40	0.46

n	1	3	5	7
fx (Hz)	0.19	0.28	0.35	0.42
fy (Hz)	0.22	0.33	0.42	------

Table 1. Comparison of analytical (left) and calculated (right) sloshing mode for a pool of dimension $l_x = 20m$, $l_y = 15m$, $h = 9m$ with $\rho = 1000kg/m^3$

For the actual pool model of Figure 1, some of the main (lower frequencies) sloshing modes are illustrated in Figure 2. The first of these modes has an eigen frequency around 0.05 Hz, so that its period might be longer than the seismic excitation duration itself. Figure 3 illustrates one of the higher order modes captured by the model, which eigen frequency occurs to be close to the pool horizontal isolation frequency.

A final check of the adequacy of the free fluid surface modelling is made by comparing the result of a full transient Computational Fluid Dynamics (CFD) with the one provided with the above-described FE model. A RANS $k-\varepsilon$ model with a Volume Of Fluid (VOF) representation for the free surface is used. The maximum wave height over the complete pool is recorded over time and the results are presented in Figure 4. The strong motion duration of the seismic excitation applied here is 20s. Both the FE and the CFD models give similar response for the whole duration of application of the load, then some differences of amplitude appear but the order of magnitude remain similar, as well as the phases. Because of the absence of significant damping in the fluid, in reality as in the models, the wave motions continue, albeit in a stabilized way, even after the end of the excitation.

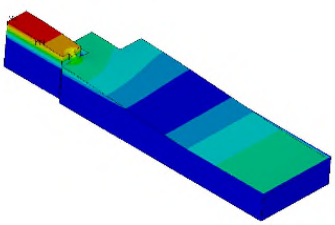

1st pure X mode

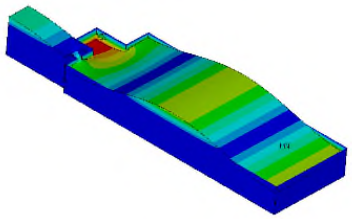

3rd pure X mode

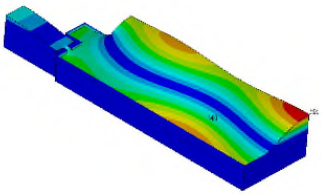

1st pure Y mode

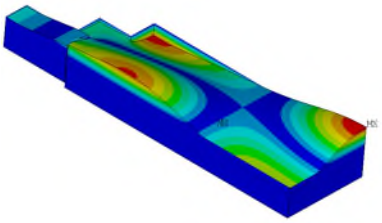

Combined X and Y mode

Figure 2. Lower order sloshing modes

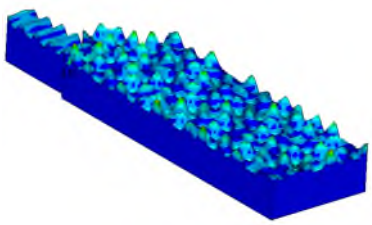

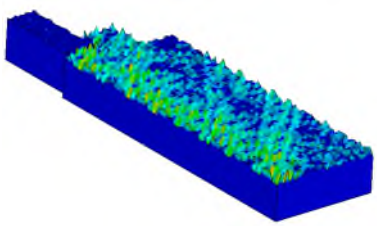

Figure 3. Higher order sloshing mode with frequencies close to the pool eigen frequency

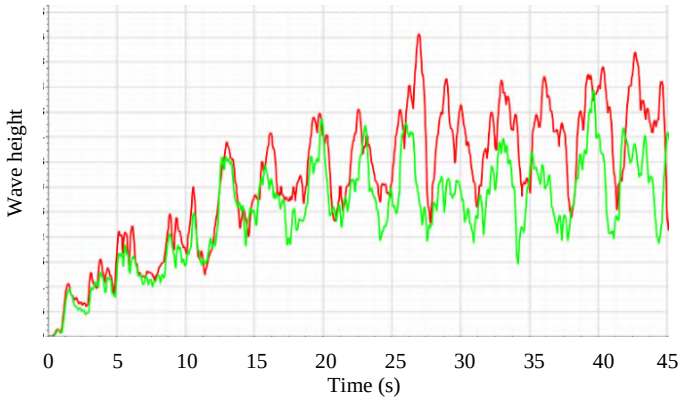

Figure 4. Comparison of FE (green) and CFD (red) results in terms of wave height response to a seismic excitation

IDENTIFICATION OF COUPLED EFFECTS

Overall view

The implementation of a seismic isolation system below a structure allows a control of its first main response frequencies, at least in the horizontal plane, and, in the case of a 3D isolation, in the vertical direction and in rocking as well. The seismic isolation system being softer than the supported structure, its main translational frequencies might be determined as the ones of a single degree of freedom system:

$$f_1 = \frac{1}{2\pi}\sqrt{\frac{K_{sis}}{M_s}} \qquad (9)$$

with K_{sis} the stiffness of the seismic isolation system and M_s the mass of the whole supported structure.

For a standard isolated structure, the participating mass of the first mode in each direction is almost equal to the total supported mass M_s, meaning that the response of the structure to a seismic excitation in this direction is almost fully determined by the response of this first mode alone. For the higher order modes, corresponding to deformations of the isolated structure, the excitation is filtered by the isolation system. The overall movement of the isolated structure is then comparable to a rigid body motion with only the isolation layer deforming. Because of the low frequency f_1 induced by the isolation system, the displacement associated to this response is generally high and dampers are included in the isolation system to limit these displacements. In-structure response spectra, used for the design of equipment within the isolated structure, are expected to show a clear peak at the isolation frequency and to flatten afterward.

In the case of a pool on an isolation system comprising damper elements, the model presented in the previous chapter has allowed to highlight several coupling effects that complicate the behavior of the structure but shall not be overseen. These are: a) cross mode coupling due to highly localised damping in the isolation system, b) fluid sloshing modes interaction with the overall dynamics, c) cross-directional coupling, here amplified by the vertical seismically induced pressure gradient in the fluid. Each of these coupling effects is presented in one of the following paragraphs, along with their consequences on the choice of analysis methodology for this kind of problem. An additional coupling effect can also appear in some applications: the coupling of acoustic modes with structural modes at frequencies that can be excited by the earthquake. For a 100 m long pool, the first acoustic mode appears at 6.5 Hz. This coupling has not been found to be predominant in the present study thanks to the filtering effect of the seismic isolation. For this reason, it is not described in the following paragraphs.

Cross mode coupling due to localized damping in the seismic isolation system

The cross-mode coupling effect, due to high localized damping in a structure, is a known phenomenon in dynamic analysis. A specific description of this phenomenon for the case of seismically isolated

structure can be found in Politopoulos 2008. The coupling arises from the fact that the $\boldsymbol{C}$ matrix in equation (1) has large components associated to the existence of localised dampers in the seismic isolation system and that this matrix, if projected into the modal basis, is not diagonal. This means that even though the higher frequency modes of the isolated structure cannot be directly excited by the earthquake, they will be excited by the first mode itself. Assuming a 2 degrees of freedom system, equation (1) projected into the modal basis $\boldsymbol{\phi}$ of the structure would become:

$$\begin{bmatrix} M_1 & 0 \\ 0 & M_2 \end{bmatrix} \begin{Bmatrix} \ddot{q}_1 \\ \ddot{q}_2 \end{Bmatrix} + \begin{bmatrix} C_1 & C_{12} \\ C_{12} & C_2 \end{bmatrix} \begin{Bmatrix} \dot{q}_1 \\ \dot{q}_2 \end{Bmatrix} + \begin{bmatrix} K_1 & 0 \\ 0 & K_2 \end{bmatrix} \begin{Bmatrix} q_1 \\ q_2 \end{Bmatrix} = - \begin{Bmatrix} \boldsymbol{\phi_1}^T \boldsymbol{M} \\ \boldsymbol{\phi_2}^T \boldsymbol{M} \end{Bmatrix} \ddot{u}_g \qquad (10)$$

with q_1, M_1 and K_1, the modal response, modal mass and modal stiffness of the first mode, corresponding to the isolated structure global rigid movement with deformation of the isolation system only, q_2, M_2 and K_2, the modal response, modal mass and modal stiffness of the second mode, corresponding to the deformation of the isolated structure and C_1, C_{12} and C_2 the terms of the non-diagonal $\boldsymbol{\phi}^T \boldsymbol{C} \boldsymbol{\phi}$ matrix. The C_{12} terms appear because the second mode does involve a deformation of the isolation system as well. Its influence on the first line of equation (10) is generally low because the C_1 term is large in comparison, corresponding to the direct effect of the damper in reducing the first mode response. On the contrary, its effect might be significant on the second line of equation (10), because the projected seismic excitation on this mode ($\boldsymbol{\phi_2}^T \boldsymbol{M} \ddot{u}_g$) is negligible and the term $C_{12}\dot{q}_1$ then acts as an external excitation on this mode.

Another way of describing the same phenomenon is that the forces transmitted by the springs to the structure are mostly low frequency and proportional to the displacement of the isolated slab relative to the ground, whereas the forces transmitted by the dampers are proportional to the relative velocity and include some higher frequency content. If the damping is high, both forces can be of the same order of magnitude. As an illustration, Figure 5 a) shows an extract of force time history in one spring and one damper and Figure 5 b) shows the Fourier spectrum amplitude of the same signals. The higher frequency excitation transmitted to the slab through the dampers is clearly visible.

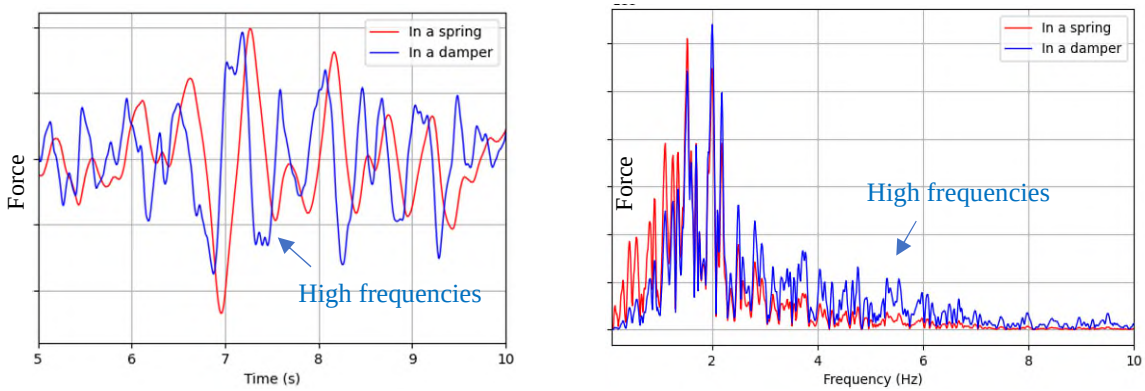

a) b)

Figure 5. Comparison of forces in a spring and a damper a) extract of time histories, b) Fourier spectrum

Because of this identified cross-mode coupling effect, it might be advised to limit the amount of damping added in an isolation system so as to ensure a sufficient control of the structure displacement without deteriorating too much the in-structure response spectra at higher frequencies. Another consequence of cross-mode coupling is that mode superposition techniques for computing the seismic response of the isolated structure tend to lose their competitive advantage in comparison with a direct solving of equation (1). In any case, if mode superposition techniques are to be used, the effect of the non-diagonal damping matrix shall be explicitly accounted for.

Fluid sloshing modes interactions with the overall dynamics

The computed fluid sloshing modes are as numerous as the nodes on the free-fluid surface of the FE model. Most of them correspond to modes like the one illustrated on Figure 3 and their frequencies span on the entire seismic excitation range. As an illustration, the free surface wave height inside the pool model subjected to a seismic excitation is given in Figure 6 for several points in time. From an initially flat fluid surface, this figure shows how the first small waves develop from the pool wall toward the pool center, how they interact with the perpendicular waves to create complex patterns of smaller waves, and finally how the main large sloshing modes become predominant after the significant time they need to reach their maximum responses.

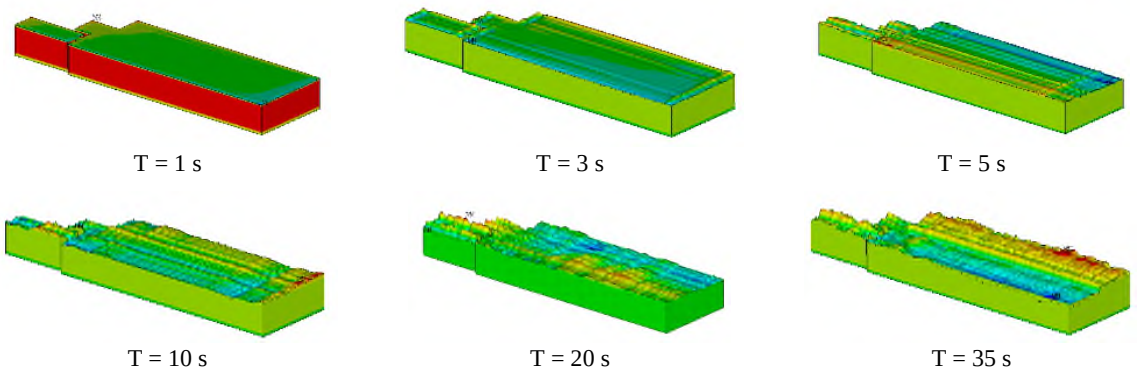

Figure 6. Seismically induced wave height at different point in time

From a wave height calculation point of view the lower as well as the higher sloshing modes may be of interest. From a structural analysis point of view, one main effect of the sloshing modes, especially those at lower frequencies, is to partially invalidate equation (9) for calculating the frequency of the isolated pool. Indeed, the mass of the fluid contained into the pool cannot be fully considered as a part of the isolated structural mass M_s in equation (9). The main sloshing modes occurring at frequencies much below the isolation frequency, their response is unaffected by the seismic isolation system and this results in part of the water mass moving in a way that is decoupled from the main pool movements. Consequently, the pool isolation frequency in each direction becomes:

$$f_1 = \frac{1}{2\pi}\sqrt{\frac{K_{sis}}{M_s - M_{slosh}}} \qquad (11)$$

with M_{slosh} the mass of water decoupled from the pool main structure response mode. The separation of the water mass into one that is “attached” to the pool and one that is “detached” from it is similar in principle to the division between convective and impulsive masses defined in the Eurocode 2008 for the structural analysis of tanks and reservoirs. Still, the Eurocode formula cannot be directly used to determine M_{slosh} because they are developed for one mode excited at a time, whereas several sloshing modes in each direction might be contributing to M_{slosh} in our case.

Cross-directional coupling and vertical pressure gradient effect

Cross directional coupling effects exist for all 3D structures submitted to an earthquake type excitation. These effects are particularly visible when deriving floor response spectra of structures supported on a standard seismic isolation system, as highlighted in Politopoulos 2011 and Moussallam 2011. In such structures, the horizontal floors response due to the horizontal excitation is dramatically reduced by the seismic isolation system. On the contrary, the horizontal response due to the vertical excitation is not reduced and can, in some cases, even be amplified by the seismic isolation system. This results in significant peaks in the horizontal spectra at the frequencies of the vertical modes. Example of structures exhibiting significant cross directional coupling are given in Figure 7 b) and c).

In the case of the storage pool, its geometry is best described by the structure illustrated in Figure 7 c). Additional to the pure structural cross direction coupling of Figure 7, the presence of the fluid inside the pool induces a cross directional coupling of its own: the main vertical response of the pool, at its vertical isolation frequency, induces the development of a vertical pressure gradient inside the fluid. In nature, this gradient is similar to the hydrostatic pressure induced by gravity. Unlike the hydrostatic pressure, this vertical pressure gradient varies in time with the same frequency as the vertical isolated response frequency. Doing so, it applies horizontal forces on the lateral walls of the pool at a frequency equal to the vertical isolation frequency. These forces act as a horizontal excitation of the walls and may even induce some resonances if the wall main mode frequencies lie close to the vertical isolation frequency.

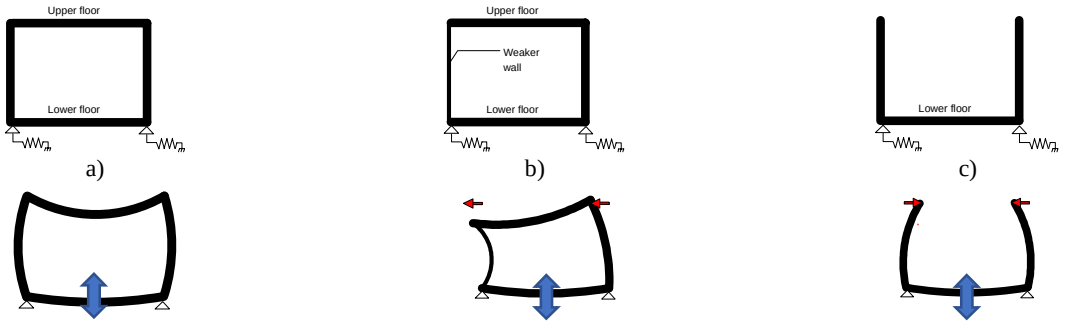

Figure 7. Typical horizontal local motions induced by global vertical response of seismically isolated structures: a) symmetrical closed frame – no coupling, b) unsymmetrical frame, c) open frame

COMPARISON TO SIMPLIFIED INDUSTRIAL METHODOLOGIES

Two simplified methodologies are often used in the industrial practice to simulate the seismic response of storage pools or tanks. In the simplest methodology, the fluid is modelled as added directional masses to the structure: masses acting vertically on the pool bottom and masses acting normal to the wall on the pool walls. A more refined methodology consists in dividing the horizontal acting water mass into an impulsive part, moving together with the wall, and a convective part, connected by springs to the structure and usually representing the first sloshing mode. The division of the water mass into impulsive and convective parts is straightforward based on the equations detailed in the Eurocodes.

For most tanks design, and for some pools of limited dimensions, representing the free fluid surface behaviour with a convective mass gives a rather good approximation of the horizontal forces on the structure resulting from the first sloshing mode, which is usually dominant. For large dimension pools, and as observed in our case, the first sloshing mode might not be the dominant one and the actual response is a combination of several sloshing modes. Using several convective masses and associated springs for each mode of importance, based on the Eurocodes formula, leads to a significant mass overestimation compared to the actual water mass: the sum of all convective masses plus the impulsive mass is not anymore equal to the water mass. This approach can be used for a pseudo-static design of a water containing structure but not for the determination of the dynamic response of the pool. Acknowledging that the impulsive and convective decomposition of the water mass is not adapted for an accurate representation of the sloshing modes in a large pool, this method does not provide any tangible advantage compared to the added mass method and will not be discussed further.

To illustrate the differences between the full fluid FE approach of the present paper and the simpler industrial approaches, floor response spectra are extracted at one node on the pool bottom corner and one node at the centre of the longitudinal lateral wall. The floor response spectra in the X (longitudinal) and Y (transversal) directions are plotted in Figure 8. Looking at the spectra in the X direction for both nodes, and in the Y direction for the corner bottom node, the shift of the horizontal isolation frequency due to the decoupling of the M_{slosh} mass in equation (11) is clearly visible. Because the horizontal isolation frequency is generally set on the increasing part of the ground response spectra,

this shift of frequency also results in an increase of amplitude of the peak and of the zero-period acceleration (max acceleration of the selected point). Looking at the spectra at the centre wall node in Y, the cross directional coupling of Figure 7 c) is visible in the fact that, whatever the method, there is not one single peak at the horizontal isolation frequency, around 1.5 Hz, but also a second peak near at 3 Hz for the fluid FE method and a prolongation of the spectral plateau to 2.7 Hz in the case of the directional added masses. In this case, 3 Hz corresponds to the vertical isolation frequency of the pool and 2.7 Hz to the first flexural mode of the longitudinal wall. In the case of the fluid FE model, it is noticeable that a very large amplification is observed compared to the added mass model. This is due to the cross-directional coupling induced by the pressure gradient due to the vertical response of the pool at 3 Hz. In the case illustrated here, representing this effect is mandatory to generate adequate floor response spectra for the analysis of components attached to the pool structure.

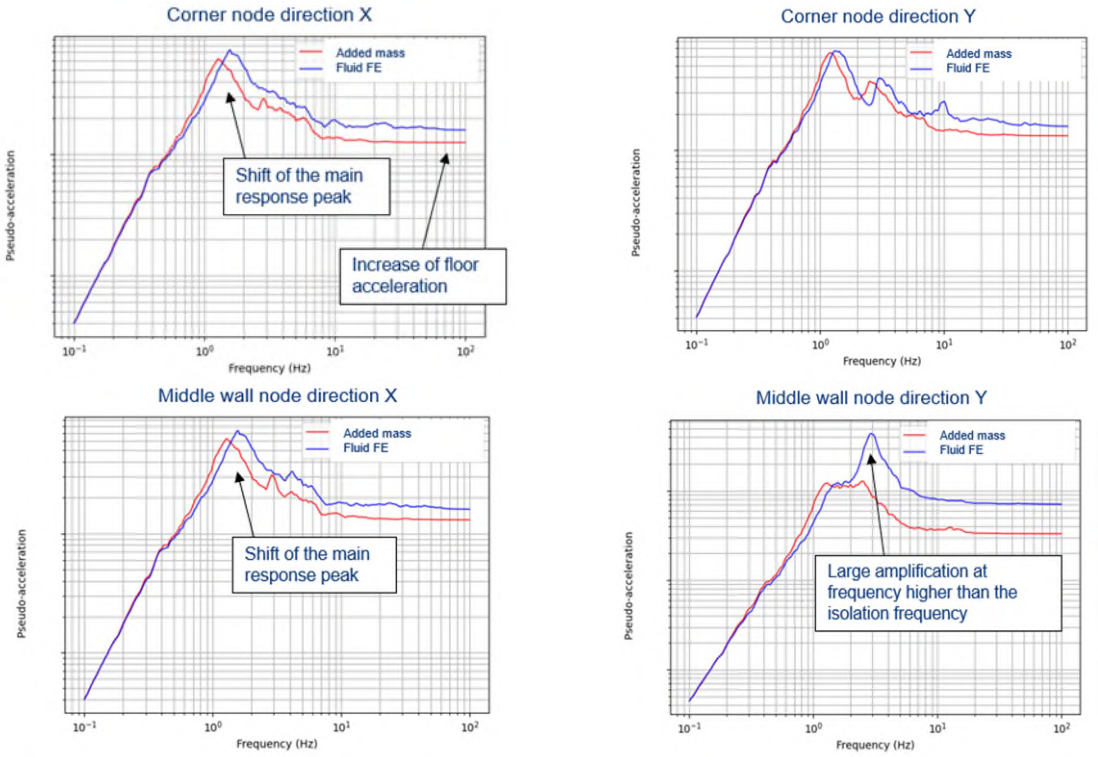

Figure 8. Comparison of response spectra with added directional mass and with full fluid-structure modelling

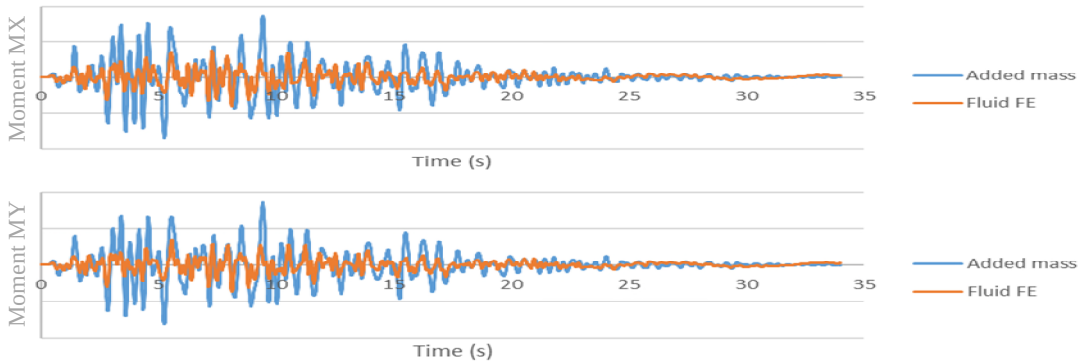

Figure 9. Comparison of bending moment at the wall to bottom connection in X and Y

Finally, the time history of dynamic moments at the mid wall connection between walls and bottom are compared in Figure 9. The static moments due to the deformation under self-weight and to the hydrostatic pressure are not included in these graphs. Even though the sloshing effect and the cross-directional coupling effect are not represented by the added mass method, the inertial forces produced

by the masses themselves on the walls tend to generate higher moments than the ones from the fluid FE model. Based on this comparison, the simple added mass method is deemed adequate for the civil design of the pool bottom and walls as it provides some additional conservatism compared to the more precise fluid FE model.

CONCLUSION

A 3D coupled fluid-structure finite element model of a seismically isolated pool was created. The main lessons learned from this model are that strong coupling phenomena occur that significantly affect the seismic response of the pool: a) cross mode coupling due to highly localised damping in the isolation system, b) fluid sloshing modes interaction with the overall dynamics, resulting especially in an increase of the first isolated mode frequency, and c) cross-directional coupling, here amplified by the vertical seismically induced pressure gradient in the fluid. Additionally, for large dimensions pools, acoustic modes are in the range of excitation frequencies of the earthquake. This effect was not predominant in the present case, thanks to the seismic isolation system, but it could become so in other applications.

To correctly determine the in-pool response spectra as well as the wave height during and after the earthquake, these coupling effects shall not be overseen, and the use of a full fluid-structure finite element model is recommended. The simpler approaches sometimes used in the industry, such as modelling the fluid as simple added mass or as impulsive and convective mass or use standard modal damping or diagonal modal damping matrices for a highly damped isolation system, would lead to incorrect in-pool response spectra. On the other side, these simpler approaches are generally conservative when determining forces and moment within the isolated structure itself.

Finally, the design of the seismic isolation system of the pool shall be made by explicitly considering the effect of both the water sloshing modes and the mode coupling due to localized damping. For this application again, the use of a full fluid-structure finite element model is recommended.

REFERENCES

AFCEN, (2014). *French Experience and Practice of Seismically Isolated Nuclear Facilities.* PTAN CR-RG-2014-02-18-1

Eurocode 8 (2007). *Design of structures for earthquake resistance – Part 4: Silos, tanks and pipelines.* EN-1998-4: 2007-03

Housner, G.W. (1957). *Dynamic Pressures on Accelerayed Fluid Containers*, Bulletin of the Seismological Society of America, vol 47, no 1, January 1957, pp15-37

Moussallam, N. and Vlaski, V. (2011), *Respective role of the vertical and horizontal components of an earthquake excitation for the determination of floor response spectra f a base isolated nuclear structure – Application to Gen IV reactors*, Transactions, SMiRT 21, 6-11 November, 2011, New Delhi, India, Div-V: Paper ID# 80

Moussallam, N., Allain, F., Petre-Lazar, I., Connesson, M., Diaz, S., Vu, T., Bouteuleux, S., Soupel, B., Labbé, P., Thiry, J.M., (2013), *Seismic Isolation of Nuclear Structures – Overview of the French Practice and Experience*. Transaction SMiRT 22, 18-23 August, San Francisco, Ca, USA, Div VI.

Nawrotzki, P., Siepe, D., Salcedo, V., (2019), *Seismic Protection of NPP Structures by 3-D Base Control Systems.* Transactions SMiRT 25, 4-9 August, Charlotte, NC, USA, Div-V.

Politopoulos, I. (2008), *A review of adverse effects of damping in seismic isolation*, Earthquake Engng Struct. Dyn. 2008; 37:447–465

Politopoulos, I., Moussallam, N., (2011), *Horizontal floor response spectra of base isolated buildings due to vertical excitation*, Earthquake Engng Struct. Dyn. 2011; 10:1002–1139